Journal of Naval Architecture and Marine Engineering
January, 2026
https://dx.doi.org/10.3329/jname.v23i1.83437 *http://www.banglajol.info*

MAGNETO-CHEMICALLY RADIATIVE MICROPOLAR NANOFLUID FLOW OVER AN INCLINED STRETCHING SHEET WITH SLIP EFFECTS

Pennelli Saila Kumari[1], Shaik Mohammed Ibrahim[2]*

[1]Research Scholar, Department of Mathematics, Koneru Lakshmaiah Education Foundation, Green Fields, Vaddeswaram, Andhra Pradesh. – 522302, India. Email address: mellacheruvu.saila@gmail.com .
[2]Department of Mathematics, Koneru Lakshmaiah Education Foundation, Green Fields, Vaddeswaram, Andhra Pradesh. – 522302, India. Email address: ibrahimsvu@gmail.com.

Abstract:

This article conducts a detailed semi-analytical study on the steady flow of micropolar nanofluid over an inclined elongating sheet under multi-slip effects. This study examines the impacts of magnetic fields, heat source, chemical reaction, thermal radiation, and momentum, thermal, and concentration slip to model real-world systems for improved heat and mass transfer in key industrial applications. Similarity transformations convert the governing equations into nonlinear Ordinary Differential Equations (ODEs). The Homotopy Analysis Method (HAM) is used for numerical solutions. The results for the micropolar nanofluid's velocity, microrotation, temperature, concentration, friction factor, and mass and thermal transmission rates are presented pictorially and analyzed quantitatively. Findings reveal that enlarging thermophoresis, thermal source, radiation, and Brownian motion factors enhance the thermal distributions of the micropolar nanofluid flow. The validity of the results is confirmed through comparison with existing literature, demonstrating strong agreement. This study provides valuable insights into non-Newtonian fluid behavior and highlights the effectiveness of HAM-based numerical techniques in solving boundary layer problems.

Keywords: Micropolar fluid, multi slip, nanofluid, inclination surface, micropolar nanofluid chemical reaction, MHD, heat generation or absorption.

NOMENCLATURE:

U_∞	Free stream velocity	A	Momentum ratio significator
u, v	Velocities in (x, y) directions	Re_x	Local Reynolds number
B_0	intensity of magnetic field	Nu_x	Local Nusselt number
Le	Lewis number	κ	Thermal conductivity of fluid
Ω	Inclined sheet angle	D_T	Thermophoresis diffusion factor
D_B	Random diffusion factor	Sh_x	Local Sherwood number
C	Fluid Concentration	T	Thermal of a fluid
C_w	solutal at the wall	T_f	Thermal of a hot fluid
C_∞	ambient concentration	T_w	Wall thermal
Nb	Random motion significator	T_∞	ambient thermal
Nt	Thermophoresis significator	$\hbar_1, \hbar_2, \hbar_3$ and $\hbar_4$	non-zero auxiliary constraints
S	Suction constraint	Pr	Prandtl number
h_f	Heat transfer factor	Q_o	Heat generation with no dimension
μ_∞	Limiting viscosity at infinite shear rate	g	gravitational acceleration
k	Material constraint	F	Similarity function for velocity
	Greek symbols	R	Thermal radiation constraint
μ	Dynamic viscosity of the fluid	$(\rho c)_p$	Volume heatcapacity
σ	electrical conductivity	$(\rho c)_f$	fluid heat capacity

1813-8535 (Print), 2070-8998 (Online) Received on: July, 2025

k^*	absorption coefficient	γ^*	Spin gradient viscosity
η	dimensionless similarity variable	K^*_1	Vertex viscosity
$\tau = \frac{(\rho c)_p}{(\rho c)_f}$	Nanofluid-to-base fluid heat capacity ratio.	δ_1	Velocity slip constraint
χ_n	Characteristic function	δ_2	Thermal slip parameter
$D_i (i = 1 \text{ to } 7)$	Arbitrary constants	Q	Heat generation factor
Gr	local Grashof number due to thermal	Gc	Local Grashof number due to solutal
σ^*	Stefan -Boltzmann constant	υ	kinematic viscosity of the fluid
	Subscripts	δ_3	Solutal slip constraint
J^*	Micro inertia per unit mass	∞	Condition at the free stream
	Sub scripts	ϕ_∞	Dimensionless solutal function at the surface
w	Condition at the surface Acknowledgements	ξ	Inclination constraint
N^*	Non-dimensional angular velocity	$-\phi'(0)$	Lessened Sherwood number
$M_1, M_2, M_3 \& M_4$	Non linear operators	MHD	Magneto-Hydrodynamics
$-\theta'(0)$	Lessened Nusselt number	HAM	Homotopy analysis method
δ_4	Micro Rotation constraint		

1. Introduction

The rate of thermal transport is a measurement that is used to determine the way heat is transmitted inside a system. Nanofluids improve heat transfer rates by virtue of enhanced convective capabilities of heat transfer and higher thermal conductivity. Nanofluids are ideal for applications requiring well-organized heat dissipation, such as cooling systems for nuclear reactors, automotive engines, and electronic devices. The idea of nanofluids is not a new one. Choi and Eastman (1995) first introduced it while exploring innovative coolants and cooling methods. Its rapid rise in fame was a result of its diverse applications in, heat exchangers, nuclear reactor systems, and energy storage devices, and electronic cooling, boilers. Within a nanofluid, there are tiny amounts of nanoparticles or nanofibers, tiny particles measuring less than 100 nm in diameter. Nanofluids are produced by blending nanoparticles or nanofibers with various heat transfer base fluids such as toluene, water, motor oil, and ethylene glycol. Eastman et al. (1996) provided the first evidence showing that nanoparticles may improve the temperature characteristics of fluids. Mintsa et al. (2009) calculated the heat transfer capacity of CuO/H_2O and Al_2O_3/H_2O nanofluids and found that conductivity improves with increasing particle volume fractions, smaller particle sizes, and higher temperatures, consistent with existing data and models. The theoretical method for studying nanofluid border sheet movement across an elongating sheet was proposed by Khan and Pop (2010).

Senthilraja et al. (2010) discussed the improved thermophysical properties of nanofluids and their possible uses as coolants, fuel substances, lubricants, dampers, and refrigerants in the automobile sector, which are covered in this study. Colangelo et al. (2010) examined the nano-fluids may improve cooling in electronic devices whose size has been reduced, emphasizing its capacity towards augment operational performance and facilitate more decrement. Recently, a few numbers of investigators Sadighi et al. (2023), Zeeshan et al. (2021), Vinod Kumar Reddy and Lakshmi Narayana(2021b), Younes et al. (2022), Soomro et al. (2018) have made main charities of nanofluids field through their examination of the subject.

Considering the growing significance in the organizational and industrial sectors, the study of unconventional fluid mechanics has attracted a significant amount of interest from the academic community. There is a connection between the different characteristics and geometry of non-Newtonian fluids and the shear force dependency and rate of the shear. Non-Newtonian substances have a vital ranging of applications involving but not limited to the following: colorants, mixed materials, coatings, polymeric solutions, wastewater effluent, clay-based concrete, and medicinal compounds. Blood, saliva, and synovial fluid are all examples of biological fluids that exhibit non-Newtonian fluid behavior. Other examples include interstitial fluid and cartilage fluid. When it comes to non-Newtonian fluids, there are a variety of well-established models that are capable of

capturing the features of these objects. The micropolar fluid paradigm is one example of such a model. This model contains a wide range of different properties and technical applications, includes animal blood, liquid crystals, and polymeric suspensions, among other things. Due to the nature of their classification, an extensive range of investigations is included.

Initially, Eringen (1996) showed that Navier-Stokes assumptions cannot adequately characterize many physiological fluids due to microscopic effects created by local structure and micromotions of their components. Such fluids include micropolar fluid. After adding thermo-micropolar fluids to his theory, Eringen (1972) created constitutive equations to characterize their behavior. Transport phenomena study can help aerodynamic plastic extrusion, blow molding, rolling, and extrusion. This information also aids water-phase condensation processing. Lukaszewicz (1999) studied micropolar fluid flow's mathematics and found that it defies Newton's equations, expanding Eringen's idea. Rana et al. (2021) worked with theoretical models to explore how microorganisms move in hot blood, a Williamson fluid, and how velocity gradients impact them in suspension. The impacts about heat energy and floating force regarding the motion of MHD micropolar nanofluids were computationally computed by Rehman et al. (2021) using an elongating/shrinking sheet that included the thermal source. Using the homotopy analysis technique, Hayat et al. (2008) inquired the steady passage of a mixed convective micropolar fluid non-linear elongating surface. This was done in order to recognize this phenomenon. Dawar et al. (2020) came up with the idea of the hydromagnetic flow of a chemically reacting micropolar nano liquid that was carried out by an expanding sheet. A computer examination of the flow of micropolar nanofluids between a configuration of parallel plates was carried out by Awan et al. (2021), incorporated the impacts of electrical magnetohydrodynamics and hall current into their investigation. Furthermore, non-Newtonian fluid motion has been the subject of contemporary research, which is illustrated in references Batool et al., (2022), Thabet et al., (2023), Patel et al., (2024), Meenakumari et al. (2024), Ibrahim et al. (2025), Rahman et al., (2010), Uddin (2011), Bhargava et al., (2007), Roja et al. (2024).

Magnetohydrodynamics, sometimes known as MHD, is a sphere of inequity that examines the behavior of conductive fluids electrically when magnetic fields are present. In conjunction with thermal radiation, viscous dissipation, and heat sources, microscopic heat transfer (MHD) investigates the loss of energy and transfer of heat in fluids. The design of cooling systems for nuclear reactors, heat control in spacecraft, and material handling in metallurgy are all areas in which this has significant importance. As a result of this, Sharma and Gandhi (2022) investigated the MHD flow rate within a plate that was positioned vertically and extended in a Darcy Forchheimer porous medium. They focused on synergistic impact of Joule heating and a thermal source or sink that was not uniform. In addition, Hasanuzzaman et al., (2023) examined the impact of fluid dissipation on the transient magneto-convective thermo-mass transmission on a vertical permeable surface that incorporates thermal radiation when the surface was subjected to thermal radiation. Through the utilization of an expanding sheet, Alamirew et al. (2024) conducted an examination on the effects that the Hall effect, ion slip, viscosity dispersion, and asymmetric radiant heat have on the dynamics of MHD Williamson nanofluids. The fluid flow through magnetohydrodynamics has been explored by the researchers Malleswari et al. (2024), Alao et al. (2024), Ajithkumar and Lakshminarayana (2023), Abo-Eldahab and Salem (2005) and Sanjana and Lavanya under a variety of different kinds of conditions.

The participation of slip is a one-of-a-kind component that minimizes resistivity in a range of engineering employments, including aerodynamics and marine ships, amongst others. The consequences of slip are typically utilized in petroleum engineering and improved oil recovery. Slip is responsible and which influences fluid movement through porous rocks, is significant. It was Navier's work that laid the groundwork for the idea of slide in the fluid dynamics domain. Research conducted by Fang et al. (2010) looked at the motion of fluids in viscous substances, whereas Ibrahim (2017) explored the slip phenomenon in non-Newtonian fluids. The utilization of porous dissipation in this work is what makes it stand out from other studies since it brings a new viewpoint on the relationship between fluid dynamics and temperature impacts. Rafique et al. (2019) prepared a model for stagnation point impact on the nanofluid mixed with micropolar through a sloping surface by using Keller box technique. The findings of this research make a substantial contribution to their respective domains, thereby giving professionals and researchers Majeed et al. (2021), Swain et al. (2023), and Swarna et al. (2024), vital insights.

In the literature, studies have been conducted on micropolar nanofluid with inclined stretched sheet. However, there has been a lack of research specifically focusing on non-Newtonian micropolar fluids in the context of inclined stretching sheet with multi slip conditions, and homogeneous reaction parameters influenced by magnetic fields and thermal radiation. This study seeks to address this research gap by examining how these

factors affect the momentum, thermal, and solutal contours, taking into account the surface which is an inclined stretched sheet with multi slip effects, With the help of the MATLAB HAM technique approach. we were able to generate computational solutions for the contours of momentum, microrotation, thermal, and mass, as well as skin friction, coupled stress, and the rates of heat and mass transmission. The findings of this study provide important insights that can be used to recover heat management systems in a variety of applications in engineering, such as the cooling of electronic devices, the efficiency of thermal exchangers, and the optimization of energy systems. It is possible for engineers to create progressive thermal systems with improved efficiency and effectiveness if they are able to elucidate the complex fluid dynamics of micropolar nanofluids. This will result in improved performance and energy savings in industrial and technological processes.

1.1 Research Question

(1) What effects do heat sources and radiation have on micropolar nanofluid boundary layer flow and thermal transmission properties?
(2) How do numerous slip effects affect the flow, temperature, and concentration profiles of micropolar nanofluids? How do Brownian movements and thermophoresis affect these profiles?
(3) When it comes to micropolar nanofluids, how may magnetohydrodynamics (MHD) affect heat transfer efficiency?
(4) In order to foretell how micropolar fluid variables would affect thermal and flow distributions, how can one make efficient use of the HAM method solver?
(5) In a micropolar nanofluid system, how do the Schmidt number and the Prandtl number affect the optimization of heat transfer and flow dynamics?

2. Mathematical Formulation

The effects of numerous slip effects and chemical reaction radiation on magnetohydrodynamic flow in a micropolar nanofluid are investigated in this work. Ignoring induced magnetic fields, a constant-strength magnetic field is applied perpendicular to the inclined surface. As seen in fig. 1, the x and y axes are aligned along and normal to the surface.The wall is stretched with momentum $U_w = ax$ along the x-axis, and the sheet is inclined at an angle Ω relative to the vertical axis. The velocity is given by $U_\infty = bx$ as $y \to \infty$ .. The temperatures far and close from the surface are represented by T_∞ and T_w respectively, while solutals are represented by C_w and C_∞ The analysis considers thermophoretic effects and random motion.

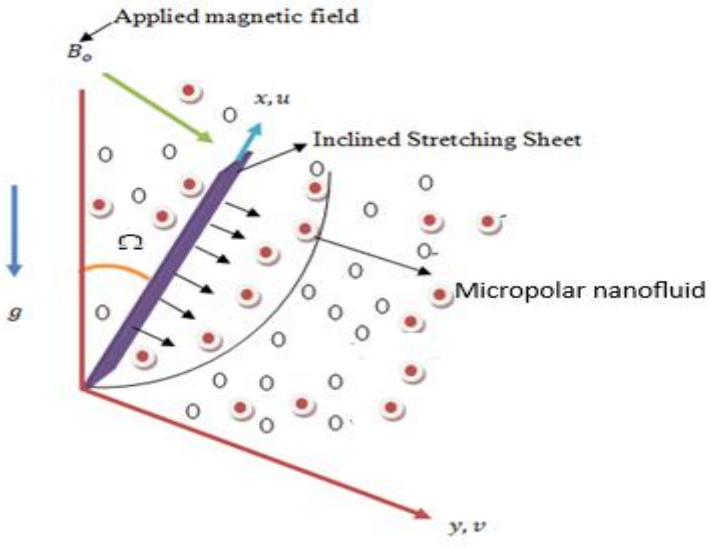

Figure 1. Coordination system and physical model

The detailed formulation of these equations is provided by Rafique et al. (2019):

$$v_y + u_x = 0\,, \tag{1}$$

$$vu_y + uu_x = u_{yy}\left(\frac{\mu_f + K_1^*}{\rho_f}\right) + N_y^*\left(\frac{K_1^*}{\rho_f}\right) - g\cos\Omega\left[-\beta_T^*\left(-T_\infty + T\right) - \beta_C^*\left(-C_\infty + C\right)\right] \tag{2}$$

$$+\frac{dU_\infty}{dx}U_\infty - \frac{B^2(x)\sigma_f}{\rho_f}\left(u - U_\infty\right),$$

$$uN_x^* + vN_y^* = \left(\frac{\gamma^*}{(j*\rho)_f}\right)N_{yy}^* - \left(\frac{K_1^*}{(j*\rho)_f}\right)\left(2N^* + \left(u_y\right)\right), \tag{3}$$

$$uT_x + vT_y = \alpha T_{yy} + \tau\left(D_B T_Y C_y + \frac{D_T}{T_\infty}(T_y)^2\right) - \frac{1}{\left(\rho C_p\right)_f}\, q_{r_y} + \frac{Q_0}{(\rho c)_f}\left(T - T_\infty\right), \tag{4}$$

$$vC_y + uC_x = D_B C_{yy} + \frac{D_T K_T}{T_\infty}T_{yy} + Kr\left(C - C_\infty\right)\cdot \tag{5}$$

For the consideration of thermal radiation, the following expressions are derived using the Rosseland approximation. The Rosseland approximation provides a simplified pattern for radiative heat transfer in a participating medium. Under this approximation, the radiative warmth fluctuation is associated to the thermal gradient, and the radiative heat flux term is expressed as (see Siegel and Howell, 1992)

$$q_r = \frac{4\sigma^*}{3k^*}\frac{\partial T^4}{\partial y}. \tag{6}$$

Using Taylor's enlargement, we can represent T^4 as

$$T^4 \cong \left(-3T_\infty{}^4 + 4T_\infty{}^3 T\right). \tag{7}$$

Equation (4) on using (6) and (7)

$$uT_x + vT_y = \left(\alpha + \frac{16\sigma^* T_\infty{}^3}{3k^*\left(\rho C_p\right)_f}\right)T_{yy} + \tau\left(D_B T_y C_y + \frac{D_T}{T_\infty}\left(T_y\right)^2\right). \tag{8}$$

Boundary settings of the flow pattern according as (Rafique et al. (2019):

$$\begin{aligned} &u = U_w\left(x\right) + \left(u_y\right)\left(1 + \frac{1}{\beta}\right)\delta_1^*;\ V_w = v; T = \delta_2^*\left(T_y\right) + T_w\left(x\right); N^* = -\delta_4 u_y \\ &C = \delta_3^*\left(C_y\right) + C_w\left(x\right) \text{ at } y = 0 \\ &u \to U_\infty; N^* \to 0; \quad C \to C_\infty; \quad T \to T_\infty \quad \text{as} \quad y \to \infty. \end{aligned} \tag{9}$$

Here present investigation, the stream function $\psi = \psi\left(x, y\right)$ can be taken in the formula

$$u = \Psi_y, v = -\Psi_x \tag{10}$$

The similarity transformations are listed below

$$u = f'(\zeta)ax, v = -f(\zeta)\sqrt{av}, \zeta = y\sqrt{\frac{a}{\nu}}, N^* = ax\sqrt{\frac{a}{\nu}}h(\zeta), \theta(\zeta)(T_w - T_\infty) + T_\infty = T, \tag{11}$$

$$\phi(\zeta)(C_w - C_\infty) + C_\infty = C$$

Equations (2) to (5) in its transmuted form, getting by applying (11), is

$$\left.\begin{aligned} &f'''(1+K) - f'^2 + Kh' + f''f + \left(Gc\phi + Gr\,\theta\right)\cos\Omega - M\ f' + A^2 + \left(A - f'\right)M = 0, \\ &h''\left(1 + \frac{K}{2}\right) - K\left(2h + f''\right) - hf' + fh' = 0, \\ &\frac{1}{\Pr}\left(1 + \left(\frac{4}{3}\right)R\right)\theta'' + Nb\phi'\theta' + f\theta' + Nt\theta'^2 + Q\theta = 0, \\ &\phi'' + Lef\phi' + \frac{Nt}{Nb}\theta'' - Le\gamma\phi = 0. \end{aligned}\right\} \tag{12}$$

Where

$$K=\frac{K_1^*}{\rho_f}\ M=\frac{\sigma_f B_0^2}{\rho_f a},\quad Gr_x=\frac{g\beta_T^*\left(T_w-T_\infty\right)x^3}{\upsilon^2},\quad Gr=\frac{Gr_x}{\mathrm{Re}_x^2},\quad Gc_x=\frac{g\beta_C^*\left(D_w-D_\infty\right)x^3}{\upsilon^2},\quad Gc=\frac{Gc_x}{\mathrm{Re}_x^2},$$

$$\mathrm{Re}_x=\frac{U_w x}{\upsilon}=\frac{ax^2}{\upsilon},\quad A=\frac{b}{a},\quad \mathrm{Pr}=\frac{\upsilon}{\alpha},\quad Nb=\frac{\tau D_B\left(D_w-D_\infty\right)}{\nu},\quad Nt=\frac{\tau D_T\left(T_w-T_\infty\right)}{\upsilon T_\infty},\quad R=\frac{4\sigma^* T_\infty^3}{k^* k},$$

$$Q=\frac{Q_0}{a\left(\rho c\right)_f},\ Sc=\frac{\upsilon}{D_B},\ \gamma=\frac{Kr}{a},\ \delta_1=\delta_1^*\sqrt{\frac{a}{\upsilon}},\ \delta_2=\delta_2^*\sqrt{\frac{a}{\upsilon}},\ \delta_3=\delta_3^*\sqrt{\frac{a}{\upsilon}},\ S=-\frac{V_w}{\sqrt{a\upsilon}}$$

Borders Conditions are

$$f(0)=S,\ f'(0)=1+\delta_1 f''(0), h(0)=-\delta_4 f''(0), \theta(0)=\left(1+\delta_2\theta'(0)\right),$$
$$\phi(0)=\left(1+\delta_3\phi'(0)\right), \tag{13}$$
$$f'(\infty)\to A,\ h(\infty)\to 0,\ \theta(\infty)\to 0, \phi(\infty)\to 0,$$

Key physical extents are given by, Local-Nusselt and Sherwood Number, Skin-Friction Factor are provided as

$$Nu_x=\frac{xq_w}{k\left(T_w-T_\infty\right)},\ Sh_x=\frac{xq_m}{D_B(D_w-D_\infty)}, C_f=\frac{\tau_w}{\rho_f U_w^2}$$

τ_w relates stress with the elongated surface, q_m relates mass warmth fluctuation, q_w relates wall warmth fluctuation, and k relates thermal conductivity are represented by

$$\tau_w=\left(\mu+K_1^*\right)\left(u_y\right)_{y=0},\ q_w=-\alpha\left(T_y\right)_{y=0},\ q_m=-D_B\left(D_y\right)_{y=0}.$$

Using dimensionless variables, we get the following in Equation (12)

$$\sqrt{\mathrm{Re}_x}D_f=(1+K)\,f''(0),\ \frac{Nu_x}{\sqrt{\mathrm{Re}_x}}=-\left(1+\frac{4}{3}R\right)\theta'(0),\ \frac{Sh_x}{\sqrt{\mathrm{Re}_x}}=-\phi'(0)\cdot$$

2.1 Methodology for solution using HAM

To obtain homotopic solutions for equations (12) with boundary conditions (13), we select initial guesses and linear operators as follows:

$$f_0(\zeta)=S+A\zeta+\left(\frac{1-A}{1+\delta_1}\right)\left(1-e^{-\zeta}\right); \mathrm{h}_0(\zeta)=-\delta_4\left(\frac{1-A}{1+\delta_1}\right)e^{-\zeta}; \theta_0(\zeta)=\frac{e^{-\zeta}}{1+\delta_2}; \phi_0(\zeta)=\frac{e^{-\zeta}}{1+\delta_3}.$$

The linear operators are designated as

$$M_1(f)=f'''-f'; M_2(h)=h"-h; M_3(\theta)=\theta"-\theta; M_4(\phi)=\phi"-\phi.$$

with the following properties

$$M_1\left(D_1+D_2e^{\zeta}+D_3e^{-\zeta}\right)=0; M_2\left(D_4e^{\zeta}+D_5e^{-\zeta}\right)=0, M_3\left(D_6e^{\zeta}+D_7e^{-\zeta}\right)=0; M_4\left(D_8e^{\zeta}+D_9e^{-\zeta}\right)=0.$$

where D_i ($i=1$ to 9) are the random coefficients.

If $s\in[0,1]$ represents embedding constraint, $\hbar_1,\hbar_2,\hbar_3$ and $\hbar_4$ represents the non-zero auxiliary constraints, then We formulate the zeroth-order distortion calculations as follows:

$$-(s-1)M_1\left(f(\zeta;s)-f_0(\zeta)\right)=s\hbar_1 N_1\left[f(\zeta;s),h(\zeta;s),\theta(\zeta;s),\phi(\zeta;s)\right], \tag{14}$$
$$-(s-1)M_2\left(h(\zeta;s)-h_0(\zeta)\right)=s\hbar_2 N_2\left[F(\zeta;s),h(\zeta;s)\right], \tag{15}$$
$$-(s-1)M_3\left(\theta(\zeta;s)-\theta_0(\zeta)\right)=s\hbar_3 N_3\left[F(\zeta;s),\theta(\zeta;s),\phi(\zeta;s)\right], \tag{16}$$
$$-(s-1)M_4\left(\phi(\zeta;s)-\phi_0(\zeta)\right)=s\hbar_4 N_4\left[F(\zeta;s),\theta(\zeta;s),\phi(\zeta;s)\right], \tag{17}$$

With boundary conditions

$$f(0;s)=S,\quad f'(0;s)=\left[1+\delta_1 f''(0)\right],\quad f'(\infty;s)=A,$$
$$h(0;s)=-\delta_4 f''(0),\quad h(\infty;s)=0,$$
$$\theta(0;s)=\left[1+\delta_2\theta'(0)\right],\quad \theta(\infty;s)=0,$$
$$\phi(0;s)=\left[1+\delta_3\phi'(0)\right],\quad \phi(\infty;s)=0,$$

$$N_1\left[f(\zeta;s),h(\zeta;s),\theta(\zeta;s),\phi(\zeta;s)\right]=(1+K)\frac{\partial^3 f(\zeta;s)}{\partial\zeta^3}+f(\zeta;s)\frac{\partial^2 f(\zeta;s)}{\partial\zeta^2}-\left(\frac{\partial f(\zeta;s)}{\partial\zeta}\right)^2+K\frac{\partial h(\zeta;s)}{\partial\zeta}+\left(Gr\theta(\zeta;s)+Gc\,\phi(\zeta;s)\right)+A^2+M\left(A-\frac{\partial f(\zeta;s)}{\partial\zeta}\right), \tag{18}$$

$$N_2\left[f(\zeta;s),h(\zeta;s)\right]=\left(1+\frac{K}{2}\right)\frac{\partial^2 h(\zeta;s)}{\partial\zeta^2}+\left(F(\zeta;s)\frac{\partial h(\zeta;s)}{\partial\zeta}+\frac{\partial f(\zeta;s)}{\partial\zeta}h(\zeta;s)\right)-K\left(2h(\zeta;s)+\frac{\partial^2 h(\zeta;s)}{\partial\zeta^2}\right), \tag{19}$$

$$N_2\left[f(\zeta;s),\theta(\zeta;s),\phi(\zeta;s)\right]=\frac{1}{\Pr}\left(1+\frac{4}{3}R\right)\frac{\partial^2\theta(\zeta;s)}{\partial\zeta^2}+\left(f(\zeta;s)\frac{\partial\theta(\zeta;s)}{\partial\zeta}\right)+Nb\frac{\partial\theta(\zeta;s)}{\partial\zeta}\frac{\partial\phi(\zeta;s)}{\partial\zeta}+Nt\left(\frac{\partial\theta(\zeta;s)}{\partial\zeta}\right)^2+Q\theta(\zeta;s), \tag{20}$$

$$N_3\left[f(\zeta;s),\theta(\zeta;s),\phi(\zeta;s)\right]=\frac{\partial^2\phi(\zeta;s)}{\partial\zeta^2}+Le\left(f(\zeta;s)\frac{\partial\phi(\zeta;s)}{\partial\zeta}\right)+\frac{Nt}{Nb}\frac{\partial^2\theta(\zeta;s)}{\partial\zeta^2}-Le\,\gamma\phi(\zeta;s), \tag{21}$$

The deformation equations of nth-order are given by:

$$M_1\left(f_n(\zeta)-\chi_n\,f_{n-1}(\zeta)\right)=\hbar_1 R_n^f(\zeta), \tag{22}$$

$$M_2\left(h_n(\zeta)-\chi_n h_{n-1}(\zeta)\right)=\hbar_1 R_n^h(\zeta), \tag{23}$$

$$M_3\left(\theta_n(\zeta)-\chi_n\theta_{n-1}(\zeta)\right)=\hbar_2 R_n^\theta(\zeta), \tag{24}$$

$$M_4\left(\phi_n(\zeta)-\chi_n\phi_{n-1}(\zeta)\right)=\hbar_3 R_n^\phi(\zeta), \tag{25}$$

Using following boundary conditions:

$$\begin{aligned} &f_n(0)=0, \quad f_n'(0)=\delta_1 F_n''(0), \quad f_n'(\infty)=0,\\ &h_n(0)=-\delta_4 f_n''(0), \quad h_n(\infty)=0,\\ &\theta_n(0)=\delta_2\theta_n'(0), \quad \theta_n(\infty)=0,\\ &\phi_n(0)=\delta_3\theta_n'(0), \quad \phi_n(\infty)=0, \end{aligned} \tag{26}$$

Here

$$R_n^f(\zeta)=(K+1)f_{n-1}'''+\sum_{i=0}^{m-1}f_{n-1-i}\,f_i'''-\sum_{i=0}^{m-1}f_{n-1-i}'\,f_i'+Kh_{n-1}'+\left(\mathrm{Gr}\theta_{n-1}+\mathrm{Gc},\phi_{n-1}\right)\cos\Omega-Mf_{n-1}'+(1-\chi_{n-1})\left(A^2-AM^*\right),$$

$$R_n^h(\zeta)=\left(1+\frac{K}{2}\right)h_{n-1}''+\sum_{i=0}^{n-1}f_{n-1-i}\,h_i'-\sum_{i=0}^{n-1}f_{n-1-i}'\,h_i-K\left(2h_{n-1}+f_{n-1}''\right),$$

$$R_n^\theta(\zeta)=\frac{1}{\Pr}\left(1+\frac{4R}{3}\right)\theta_{n-1}''+\sum_{i=0}^{n-1}f_{n-1-i}\,\theta_i'+Nb\sum_{i=0}^{n-1}\theta'_{n-1-i}\,\phi_i'+Nt\sum_{i=0}^{n-1}\theta'_{n-1-i}\,\theta_i'+Q\theta_{n-1},$$

$$R_n^\phi(\zeta)=\phi_{n-1}''+Le\left(\sum_{i=0}^{n-1}f_{n-1-i}\,\phi_i'-\gamma\phi\right)+\frac{Nt}{Nb}\theta_{n-1}'',$$

$$\chi_n = \begin{cases} 0, & n \le 1, \\ 1, & n > 1. \end{cases}$$

2.2 HAM convergence

The assisting factors $\hbar_1, \hbar_2, \hbar_3 \& \hbar_4$ significantly impact the convergence and accuracy of the series solutions. Therefore, $\hbar$-curves are plotted in Fig 2 to determine the valid range of parameters. We can determine from such a thorough review that the main constraint paradigm is all about $[-1.32, 0.0]$. For $\hbar_1 = \hbar_2 = \hbar_3 = \hbar_4 = -0.87$, the sequence resolutions are convergent across the entire ζ area. The convergence of the technique is indicated by Table 1.

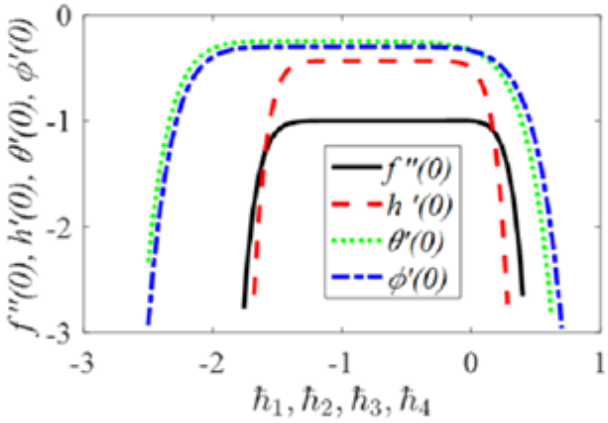

Fig. 2: Effect of $\hbar$ on $f''(0), h'(0), \theta'(0), \phi'(0)$.

Table 1. Convergence of HAM solution for various relative orders when $R = 0.5, S = A = \delta_1 = \delta_2 = \delta_3 = \delta_4 = Gr = Q = Gc == Nb = M = Nt = 0.1, K = 0.5, \gamma = 0.2,$ $\Pr = 6.5, \Omega = 60^o, Le = 5.0,$

Order	$-f''(0)$	$-h'(0)$	$-\theta'(0)$	$-\varphi'(0)$
5	1.644803	1.644803	0.845516	0.867628
10	1.644659	1.644659	0.843505	0.870935
15	1.644659	1.644659	0.843487	0.871042
20	1.644659	1.644659	0.843488	0.871025
25	1.644659	1.644659	0.843488	0.871025
30	1.644659	1.644659	0.843488	0.871025
35	1.644659	1.644659	0.843488	0.871025
40	1.644659	1.644659	0.843488	0.871025

3. Results and Discussions

Table 2: Compare of $-\phi'(0)$ and $-\theta'(0)$ for dissimilar values of Nt and Nb with $Le = \Pr = 10, \Omega = 90^o$ and in the nonappearance of leftover constraints.

Nb	Nt	Rafique et al. (2019)		Khan and Pop (2010)		Current Outcomes	
		$-\theta'(0)$	$-\phi'(0)$	$-\theta'(0)$	$-\phi'(0)$	$-\theta'(0)$	$-\phi'(0)$
0.1	0.1	0.9524	2.1294	0.9524	2.1294	0.952363	2.129288
0.2	0.2	0.3654	2.5152	0.3654	2.5152	0.365358	2.515103
0.3	0.3	0.1355	2.6088	0.1355	2.6088	0.135517	2.608694
0.4	0.4	0.0495	2.6038	0.0495	2.6038	0.049467	2.603719
0.5	0.5	0.0179	2.5731	0.0179	2.5731	0.017924	2.572978

The significance of the magnetic field and heat radiation on the movement of micropolar nanofluid over a two-dimensional inclined elongated sheet is studied using the HAM technique. The results of this investigation provide important information about how key physical parameters affect the momentum, thermal and solutal distributions and how these constraints affect the Nusselt, Sherwood number, skin-friction factor. The numerical

results gained from the numerical Bernoulli wavelet technique can be verified by comparing them with the results already published in the literature (for further details, see Table 2).

Given the high degree of agreement observed, it can be said that the suggested numerical method is accurate and trustworthy. This method can effectively solve the challenging nonlinear boundary layer equations, proving that it is appropriate for solving issues that are comparable to fluid dynamics problems.
While certain parameters are permanent, others can be changed, including
$R = 0.5, \delta_1 = \delta_2 = \delta_3 = \delta_4 = S = Q = A = Gc = Gr = Nb = Nt = M = 0.1,\ K = 0.5,$
$\Omega = 60^o, \Pr = 6.5, \gamma = 0.2 Le = 5.0.$

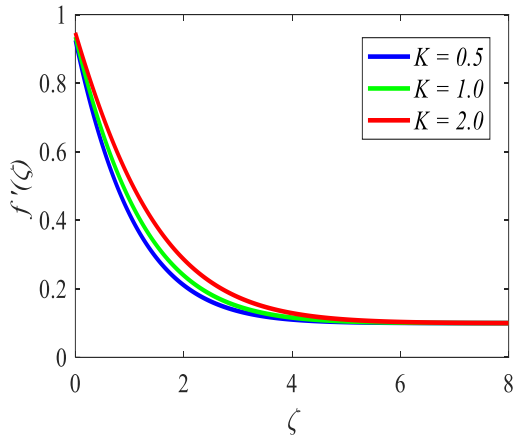

Fig. 3: Effect of ζ on $f'(\zeta)$ for different values of *K*

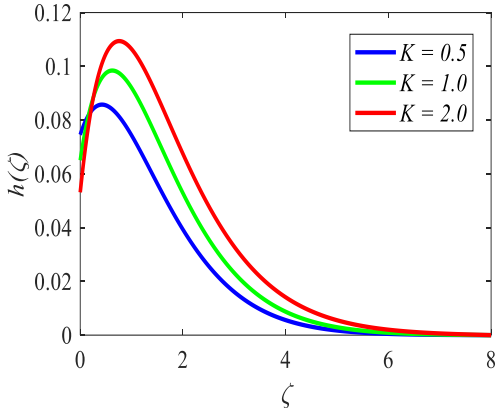

Fig. 4: Effect of ζ on $h(\zeta)$ for different values of *K*.

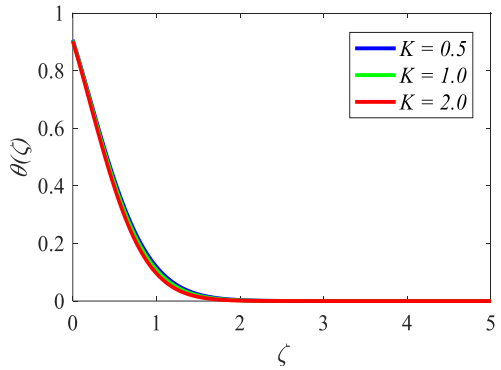

Fig. 5: Effect of ζ on $\theta(\zeta)$ for different values of *K*.

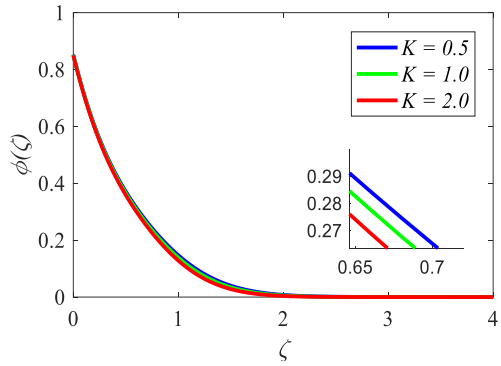

Fig. 6: Effect of ζ on $\phi(\zeta)$ for different values of *K*.

The value of K in micropolar fluids reflects the impact on velocity $f'(\zeta)$, micro rotation $h(\zeta)$, thermal $\theta(\zeta)$ and concentration $\phi(\zeta)$ contour, which is deployed in Figures 3-6. Whenever values of K get enlarged the contours of momentum and micro-rotation gets improved but on the other hand thermal and concentration contour must declines. The micropolar fluidity constraint (K) is the actual name of the material limitation that can impact the velocity outline in micropolar fluids. Here the fluidity of the micropolar limitation (K) grows, the fluid flow is more strongly influenced by the internal degrees of freedom or the microstructure.

The significance of the magnetic field limitation (M) on the momentum contour is seen in Figure 7. The momentum outline decays as the values of M upsurges. When an overflow field was imposed by a magnetic field, the Lorentz force became active. This force is strong enough to diminish the fluid flow to its momentum and drag it. Thus, fluid movement of the momentum declines as the swiftness sheet width upsurges. Figure 8 shows that when the distance from the surface increases, the value of (M) upsurges the microrotation, which is represented by $h(\zeta)$ declines. In additional words, the value of M is prolonged, the micro-rotation declines close the surface and upsurges farther away from the surface.

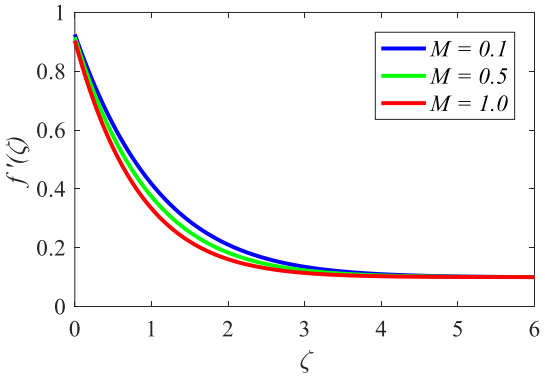

Fig. 7: Effect of ζ on $f'(\zeta)$ for different values of *M*.

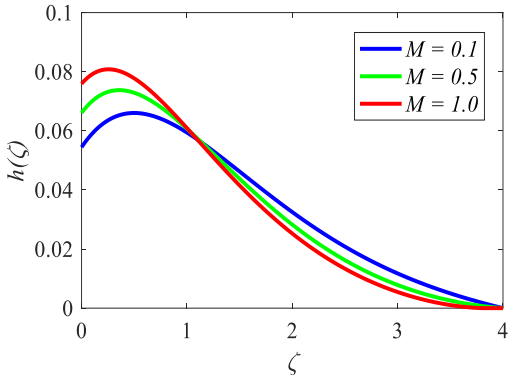

Fig.8: Effect of ζ on $h(\zeta)$ for different values of *M*.

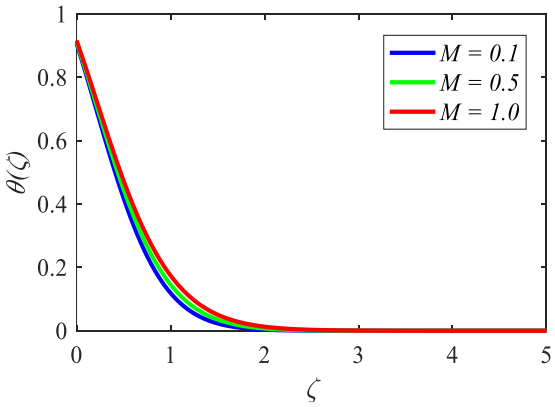

Fig.9: Effect of ζ on $\theta(\zeta)$ for different values of *M*.

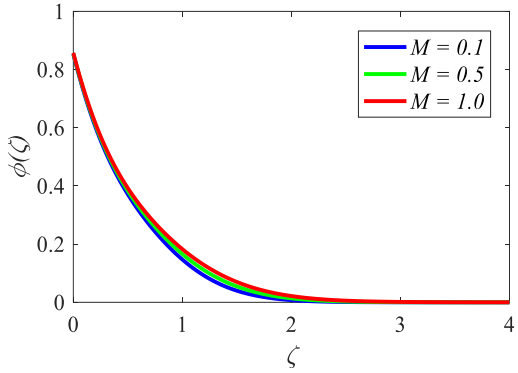

Fig.10: Effect of ζ on $\phi(\zeta)$ for different values of *M*.

The impacts of magnetic field constraint on flow thermal and solutal are displayed through Figs 9-10. From the figures, we have supposed that as magnetic field upsurges thermal and solutal contours established the behaviour of growing. Lorentz force-induced heating thickens thermal and solutal boundary layers under stronger magnetic fields.

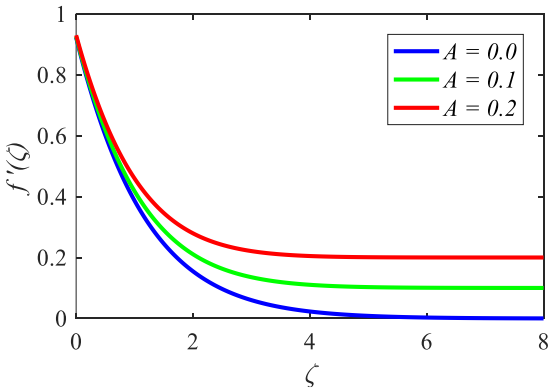

Fig.11: Effect of ζ on $f'(\zeta)$ for different values of *A*.

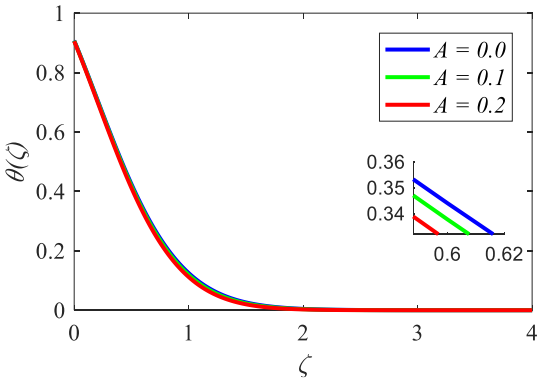

Fig.12: Effect of ζ on $\theta(\zeta)$ for different values of *A*.

Figure 11 exhibits the evolution of the swiftness curve with no dimension having different A values. As the edge film gets closer to the wall, its fluid velocity decreases, and as it moves farther away, it flows. A wall momentum that is greater than the free stream momentum is indicated by a smaller A value. Because wall inertia encourages the mutual fluid in the edge film, the fluid's speed originally decays as it gets closer to the wall. However, at a certain distance from the wall, the fluid experiences a local acceleration, which could cause the local velocity to fall below the free stream momentum. The free stream velocity then wears down the slower-moving fluid, increasing the velocity. When A equals 0, the fluid organises and does not experience the pulling impact of the free stream, as seen in Figure 11. Actually, at this point, the free stream velocity is almost

zero. The local momentum outside the boundary sheet is rushed by the free stream's boring effect for all values of $A > 0$. The discrepancy between the thermal outline and a change in momentum ratio significator A values is discovered in Figure 12. It shows that the thermal boundary sheet width declines as the momentum ratio significator upsurges. Furthermore, as A upsurges, the surface thermal upsurges (in absolute value). Thermal contour thus declines. The effect of velocity ratio significator A on the solutal graph is seen in Figure 13. The concentration boundary film thickness declines as A values upsurges. Furthermore, the graph specifies that the amount of heat on a plate's surface upsurges as A upsurges.

Figure 14 reveals the decreasing presentation of momentum for enlarged significator values, explicitly inclined angle Ω .The fluid flow converts hard because in presence of Lorentz forces, which drops the fluid's swiftness. Figure 15 clearly reveals the influence of the slip constraint δ_1 on the swiftness contour, showing a consistent reduction in swiftness as the slip constraint δ_1 increases. This phenomenon can be attributed to the direct relationship between the slip constraint δ_1 and dynamic viscosity, where larger values of α correspond to increased viscosity, ultimately resulting in reduced fluid motion.

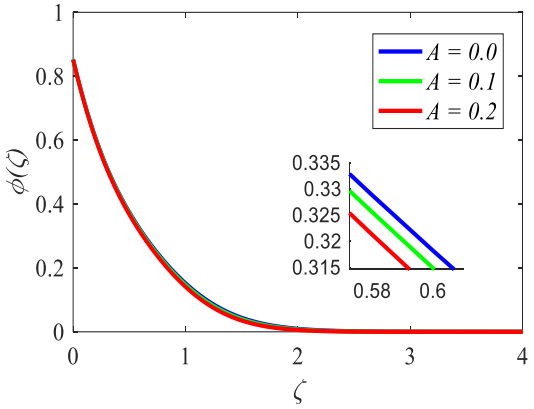

Fig.13: Effect of ζ on $\phi(\zeta)$ for different values of *A*.

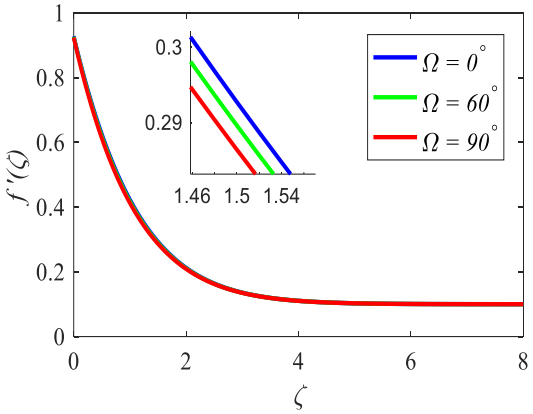

Fig.14: Effect of ζ on $f'(\zeta)$ for different values of Ω .

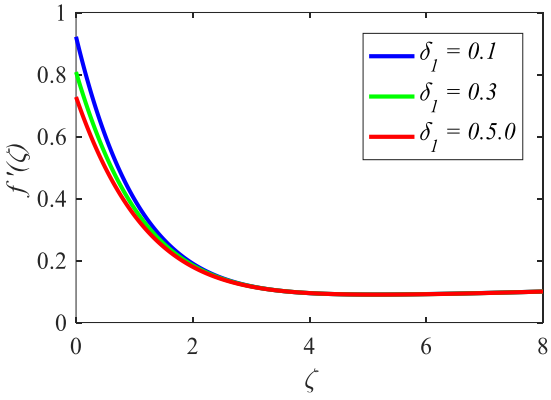

Fig.15: Effect of ζ on $f'(\zeta)$ for different values of δ_1 .

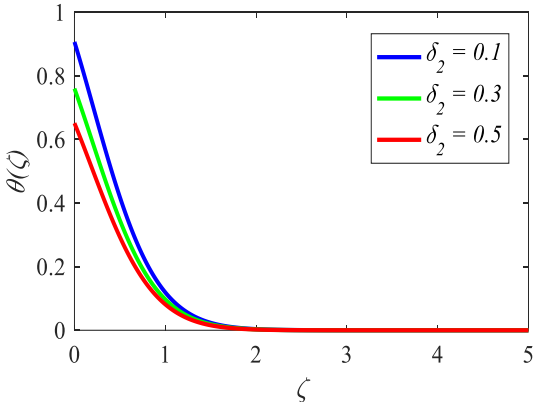

Fig.16: Effect of ζ on $\theta(\zeta)$ for different values of δ_2 .

The influence of the temperature and solutal slip constraints (δ_2 & δ_3) on the temperature and solutal contours is illustrated in Figures 16 and 17, correspondingly. As the values of the slip constraints upsurge, a notable reduction is noticed in both temperature and concentration contours. The decrease in temperature occurs because the thermal energy supplied by the hot fluid beneath the stretched sheet becomes limited. Since this thermal energy is indirectly proportional to the temperature, an upsurge in the thermal slip constraint results in a decline in temperature until it eventually stabilizes. Figure 18 shows that rising radiation parameters intensify fluid radiant energy, causing greater absorption. These actions enhance fluid heat, increasing its temperature. Figure 19 strategized the impact of the heat generation/absorption significator on thermal outlines. As the heat generation constraint increases, the thermal contours also up surges indicating a rise in the fluid's thermal state due to enhanced heat generation.

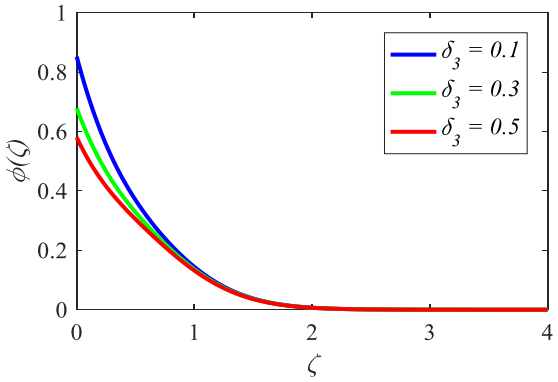

Fig.17: Effect of ζ on $\phi(\zeta)$ for different values of δ_3.

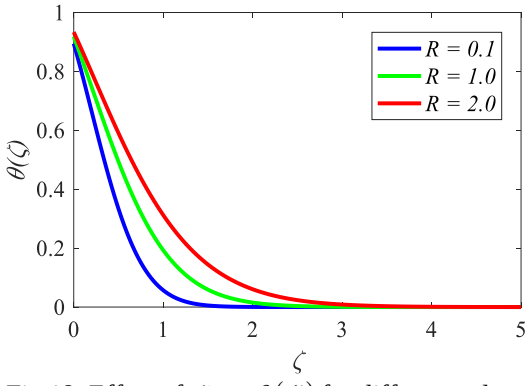

Fig.18: Effect of ζ on $\theta(\zeta)$ for different values of *R*.

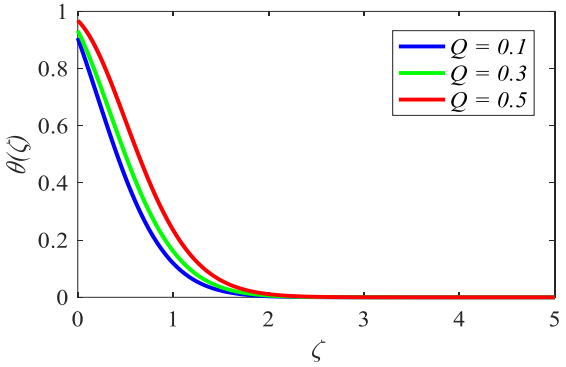

Fig.19: Effect of ζ on $\theta(\zeta)$ for different values of *Q*.

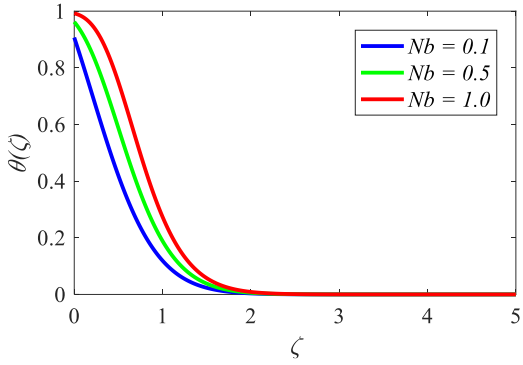

Fig.20: Effect of ζ on $\theta(\zeta)$ for different values of *Nb*.

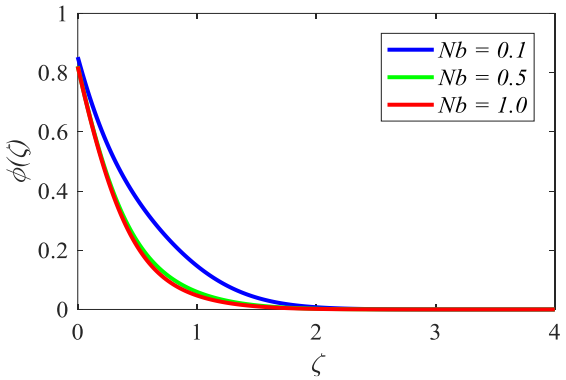

Fig.21: Effect of ζ on $\phi(\zeta)$ for different values of *Nb*.

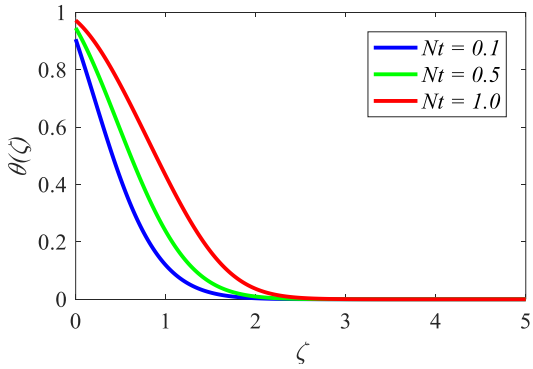

Fig.22: Effect of ζ on $\theta(\zeta)$ for different values of *Nt*.

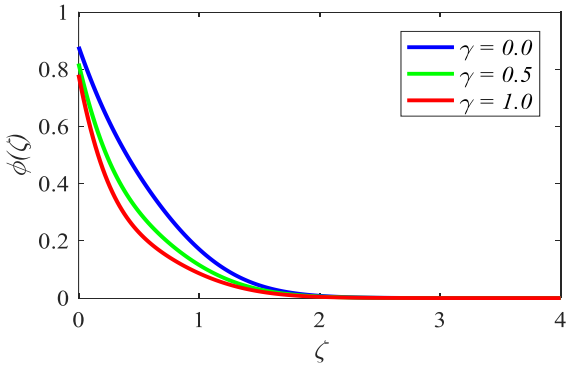

Fig.23: Effect of ζ on $\phi(\zeta)$ for different values of γ.

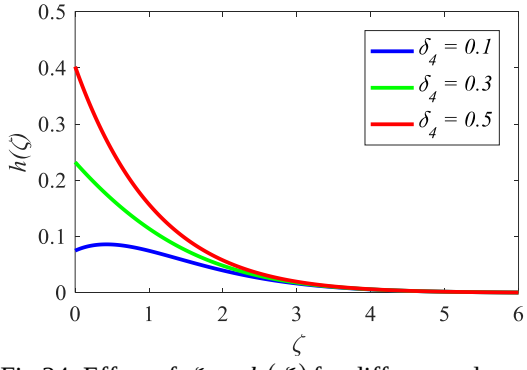

Fig.24: Effect of ζ on $h(\zeta)$ for different values of δ_4

Figures 20 and 21 depict the impact of the random motion constraint on thermal and solutal contours. Increasing the random motion constraint enhances the thermal boundary layer thickness while decreasing the thermal gradient at the surface. Conversely, the solutal contours and solutal boundary layer thickness exhibit an opposite trend, decreasing with increasing random motion constraint.

Figure 22 is portrayed to validate the effect of thermophoresis significator on thermal contour. when thermophoresis significator growths, there is an enhancement of the temperature boundary sheet thickness. Figure 23 portrayed the effect of a chemical reaction factor on $\phi(\zeta)$. It is recognized that the solutal declines as the chemical reaction significator upsurges. A variation in the angular swiftness δ_4 is portrayed in fig 24, which illustrates the solutal of micro-elements upsurges with snowballing values. When the value of δ_4 is increased, which means that the concentration of the micro-element is decreased, the micro-rotation profile is improved.

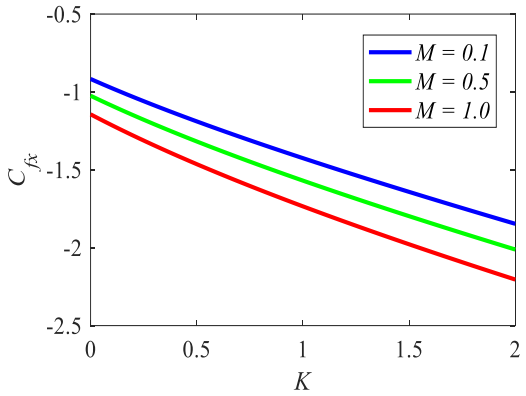

Fig.25: Effect of C_{fx} for different values of *K* and *M*.

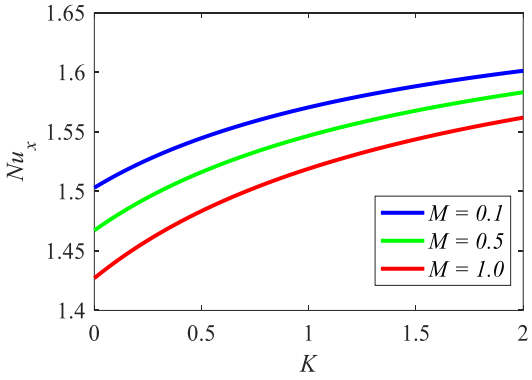

Fig.26: Effect of Nu_x for different values of *K* and *M*.

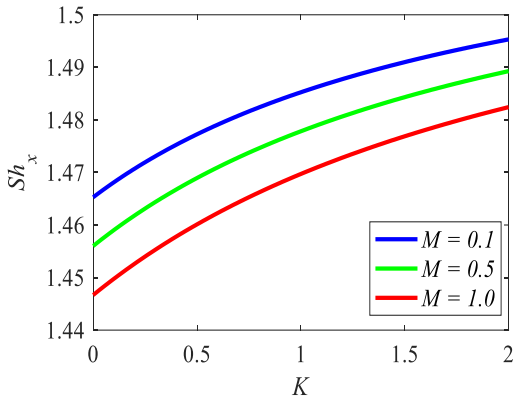

Fig.27: Effect of Sh_x for different values of *K* and *M*..

Figure 25 shows the skin-friction factor on variations of *K* and *M*. It's noticed that as *M* and *K* enlarged, the skin-friction factor decreases. In Figure 26, it is noticed that Nusselt number decays for upsurge together the parameters M and *K*. In Figure 27, it is noticed that local Sherwood number decays for upsurge together the constraints *M* and *K*.

Finally, these results emphasize the critical roles of various physical parameters in optimizing fluid behavior and transport processes across different applications. The micropolar fluid parameter is essential in industrial processes like polymer extrusion and coating, ensuring controlled flow properties for uniform product quality and efficient processing. The magnetic field significantly influences fluid dynamics, making it relevant for MHD power generation, electromagnetic flow control, and cooling systems. The Prandtl number governs heat transfer, with higher values enhancing thermal resistance, restricting heat diffusion, and leading to a more localized temperature distribution. Similarly, the stretching ratio plays a crucial role in both thermal and mass

transport, where higher stretching rates increase heat generation, enhance thermal energy accumulation, and facilitate outward solute diffusion, reducing the concentration boundary layer thickness. Additionally, the temperature exponent controls thermal energy distribution, with higher values leading to increased heat accumulation and stronger temperature gradients. Collectively, these insights offer insightful advice on how to maximise heat and mass transmission in engineering, scientific, and industrial utilizations.

4. Conclusions

An innovative enquiry of the steady radiative movement field of chemically reactive micropolar nano-material generated above a slope stretching sheet is conducted. The governing Navier-Stokes, angular velocity, energy and mass equations are addressed utilizing a compact semi-analytical (HAM) technique. This object fills the gap of the movement of micro polar nanofluid produced by the linear elongating inclined slip under multi slip effects. This is essential part in the heat and mass transfer methods in cooling systems and industry. Results are discussed through various graphical structures and core findings are listed below:

- Increasing magnetic, inclination angle, and velocity slip parameters generally reduce velocity due to stronger Lorentz force, higher resistance in flow, and flow slip forces from motion.
- Temperature profiles increase with higher magnetic and radiation parameters but decrease with increased velocity ratio, thermal slip, and Prandtl number.
- Concentration profiles decrease with higher chemical reaction and Lewis number due to faster consumption of reactive species and reduced mass diffusivity.
- Angular momentum profiles increase with higher material parameter, and magnetic field constraint.
- Skin friction decreasing with higher material constraint and magnetic field strength. The Nusselt number increases with higher material constraint and decreasing with magnetic field strength, while the Sherwood number decreases under similar conditions.
- The Thermophoresis and Brownian motion constraints exhibit reciprocal behavior.

The Homotopy Analysis Technique (HAM) used in this study accurately predicts nanofluid velocity and temperature profiles, effectively handling nonlinear differential equations and complex fluid behaviours under various conditions, ensuring reliable results.

The results highlight the promise of nanofluids, especially graphene oxide-based ones, for applications demanding efficient heat transfer and flow dynamics, including cooling systems, thermal energy storage, and industrial processes.

Future studies should explore the impact of varying nanoparticle concentrations, base fluids, and flow conditions to further optimize nanofluid performance in practical applications.

References

Abo-Eldahab, E. M., and Salem, A. M. (2005). MHD flow and heat transfer of non-Newtonian power-law fluid with diffusion and chemical reaction on a moving cylinder. Heat and Mass Transfer, 41, 703-708.

Ajithkumar, M. and Lakshminarayana, P., (2023). MHD peristaltic flow of chemically reactive Casson nanofluid in a nonuniform porous inclined flexible channel with cross-diffusion effects. International Journal of Modern Physics B, 37(25), p.2350292. https://doi.org/10.1142/s0217979223502922

Alamirew, W. D., Zergaw, G. A., and Gorfie, E. H. (2024). Effects of Hall, ion slip, viscous dissipation and nonlinear thermal radiation on MHD Williamson nanofluid flow past a stretching sheet. International Journal of Thermofluids, 22, 100646. https://doi.org/10.1016/j.ijft.2024.100646

Alao, S, S. O. Salawu, R. A. Oderinu, A. A. Oyewumi, and E. I. Akinola (2024) Investigation of thermal radiation and viscous heating effects on the hydromagnetic reacting micropolar fluid species flowing past a stretchy plate in permeable media, Int. J. Thermofluids, vol. 22, pp. 100600. https://doi.org/10.1016/j.ijft.2024.100600

Awan, S. E ,M. A. Z. Raja, F. Gul, Z. A. Khan, A. Mehmood, and M. Shoaib (2021). Numerical computing paradigm for investigation of micropolar nanofluid flow between parallel plates system with impact of electrical MHD and Hall current, Arab. J. Sci. Eng., vol. 46, pp. 645–662. https://doi.org/10.1007/s13369-020-05006-7

Batool, S. G. Rasool, N. Alshammari, I. Khan, H. Kaneez, and N. Hamadneh (2022). Numerical analysis of heat and mass transfer in micropolar nanofluids flow through lid-driven cavity: Finite volume approach, Case Stud. Thermal Eng., vol. 37, pp. 102233. https://doi.org/10.1016/j.csite.2022.102233

Bhargava, R., Sharma, S., Takhar, H. S. S., Bég, O. A. A., and Bhargava, P. (2007). Numerical solutions for micropolar transport phenomena over a nonlinear stretching sheet. Nonlinear analysis: modelling and control, 12(1), 45-63. https://doi.org/10.15388/NA.2007.12.1.14721

Choi, S. U., and Eastman, J. A. (1995). Enhancing thermal conductivity of fluids with nanoparticles (No. ANL/MSD/CP-84938; CONF-951135-29). Argonne National Lab.(ANL), Argonne, IL (United States). W-31109-ENG-38
Colangelo, G., Favale, E., Milanese, M., de Risi, A., and Laforgia, D. (2017). Cooling of electronic devices: Nanofluids contribution. Applied Thermal Engineering, 127, 421-435. https://doi.org/10.1016/j.applthermaleng.2017.08.042
Dawar A. Z. Shah, P. Kumam, H. Alrabaiah, W. Khan, S. Islam, and N. Shaheen. (2020). Chemically reactive MHD micropolar nanofluid flow with velocity slips and variable heat source/sink, Sci. Rep., vol. 10, no. 1, pp. 20926, https://doi.org/10.1038/s41598-020-77615-9
Eastman, J. A., Choi, U. S., Li, S., Thompson, L. J., and Lee, S. (1996). Enhanced thermal conductivity through the development of nanofluids. MRS Online Proceedings Library (OPL), 457, 3. https://doi.org/10.1557/PROC-457-3
Eringen, A.C. (1996). Theory of micropolar fluids. J. Math. Mech. 16, 1–8.
Eringen, A.C. (1972).Theory of thermomicrofluids. J. Math. Anal. Appl. 38, 480–496. https://doi.org/10.1016/0022-247X(72)90106-0
Fang, T., Yao, S., Zhang, J., and Aziz, A. (2010). Viscous flow over a shrinking sheet with a second order slip flow model. Communications in Nonlinear Science and Numerical Simulation, 15(7), 1831-1842. https://doi.org/10.1016/j.cnsns.2009.07.017
Hasanuzzaman M, S. Akter, S. Sharin, M. M. Hossain, A. Miyara, and M. A. Hossain (2023). Viscous dissipation effect on unsteady magneto-convective heat-mass transport passing in a vertical porous plate with thermal radiation, Heliyon, vol. 9, no. 3, pp. e14614.
Hayat T. Z. Abbas, and T. Javed (2008). Mixed convection flow of a micropolar fluid over a non-linearly stretching sheet," Phys. Lett. A, vol. 372, no. 5, pp. 637–647. https://doi.org/10.1016/j.physleta.2007.08.006.
Ibrahim, W. (2017). MHD boundary layer flow and heat transfer of micropolar fluid past a stretching sheet with second order slip. Journal of the Brazilian Society of Mechanical Sciences and Engineering, 39(3), 791-799.
Ibrahim S M, Lavanya, B., Dharmaiah, G., Sankar Reddy, T., Roja, P. (2025) Melting heat transfer effects on MHD chemically thermally radiative micropolar fluid flow towards stretching exponentially sheet with heat sink/source, CFD Letters, 17(7), 113-129, https://doi.org/10.37934/cfdl.17.7.113129
Khan, W. A., and Pop, I. (2010). Boundary-layer flow of a nanofluid past a stretching sheet. International journal of heat and mass transfer, 53(11-12), 2477-2483. https://doi.org/10.1016/j.ijheatmasstransfer.2010.01.032
Lukaszewicz, G. Micropolar Fluids: Theory and Applications; Springer Science and Business Media: Berlin/Heidelberg, Germany, 1999.
Majeed, A. H., Mahmood, R., Abbasi, W. S., and Usman, K. (2021). Numerical computation of MHD thermal flow of cross model over an elliptic cylinder: reduction of forces via thickness ratio. Mathematical Problems in Engineering, 2021(1), 2550440. https://doi.org/10.1155/2021/2550440
Malleswari, K., Nath, J. M., Reddy, M. V., Mala, M. S., and Dey, B. (2024). Thermal performance of Cattaneo-Christov heat flux in MHD radiative flow of Williamson nanofluid containing motile microorganisms and arrhenius activation energy. Journal of Computational and Theoretical Transport, 1-23. https://doi.org/10.1080/23324309.2024.2419007
Meenakumari, R., Sucharitha, G., Pallavarapu, L. and Vajravelu, K. (2024). Darcy-Forchheimer flow of a conducting micropolar fluid at a stretching sheet with convective boundary conditions. Journal of Porous Media, 27(5). https://doi.org/10.1615/jpormedia.2023045629
Mintsa, H. A., Roy, G., Nguyen, C. T., and Doucet, D. (2009). New temperature dependent thermal conductivity data for water-based nanofluids. International Journal of Thermal Sciences, 48(2), 363-371. https://doi.org/10.1016/j.ijthermalsci.2008.03.009
Priyadharshini, P., and Karpagam, V. (2024). Biomedical advantages of magnetohydrodynamics Williamson nanofluid: optimization of multiple linear regression and multilayer perceptron. Journal of Nanofluids, 13(6), 1350-1363. https://doi.org/10.1016/j.ijft.2023.100646
Patel, H., Mittal, A., and Nagar, T. (2024). Effect of magnetic field on unsteady mixed convection micropolar nanofluid flow in the presence of non-uniform heat source/sink. International Journal of Ambient Energy, 45(1), 2266748. https://doi.org/10.1080/01430750.2023.2266748
Rafique, K., Anwar, M. I., Misiran, M., Khan, I., Seikh, A. H., Sherif, E. S. M., and Nisar, K. S. (2019). Numerical analysis with Keller-box scheme for stagnation point effect on flow of micropolar nanofluid over an inclined surface. Symmetry, 11(11), 1379.
Rahman, M. M., Aziz, A., and Al-Lawatia, M. A. (2010). Heat transfer in micropolar fluid along an inclined permeable plate with variable fluid properties. International Journal of Thermal Sciences, 49(6), 993-1002. https://doi.org/10.1016/j.ijthermalsci.2010.01.002

Rana, B. M. J., Arifuzzaman, S. M., Islam, S., Reza-E-Rabbi, S., Al-Mamun, A., Mazumder, M., and Khan, M. S. (2021). Swimming of microbes in blood flow of nano-bioconvective Williamson fluid. Thermal Science and Engineering Progress, 25, 101018. https://doi.org/10.1016/j.tsep.2021.101018
Rehman, S. U., Mariam, A., Ullah, A., Asjad, M. I., Bajuri, M. Y., Pansera, B. A., and Ahmadian, A. (2021). Numerical computation of buoyancy and radiation effects on MHD micropolar nanofluid flow over a stretching/shrinking sheet with heat source. Case Studies in Thermal Engineering, 25, 100867. https://doi.org/10.1016/j.csite.2021.100867
Sadighi, S., Afshar, H., Jabbari, M., and Ashtiani, H. A. D. (2023). Heat and mass transfer for MHD nanofluid flow on a porous stretching sheet with prescribed boundary conditions. Case Studies in Thermal Engineering, 49, 103345. https://doi.org/10.1016/j.csite.2023.103345
Sanjana, T.D., and Lavanya, B. (2025). Convective heat and mass transfer in three-dimensional MHD casson nanofluid flow over an exponentially stretching porous sheet with thermal radiation and chemical reaction. Global and stochastic analysis, 12(1). 121-130.
Senthilraja, S., Karthikeyan, M., and Gangadevi, R. (2010). Nanofluid applications in future automobiles: comprehensive review of existing data. Nano-Micro Letters, 2(4), 306-310. https://doi.org/10.3786/nml.v2i4.p306-310
Sharma, B. K., and Gandhi, R. (2022). Combined effects of Joule heating and non-uniform heat source/sink on unsteady MHD mixed convective flow over a vertical stretching surface embedded in a Darcy-Forchheimer porous medium. Propulsion and Power Research, 11(2), 276-292. https://doi.org/10.1016/j.jppr.2022.06.001
Siegel, R., and Howell, J. R. (1992). Thermal Radiation Heat Transfer. Hemisphere Publishing Corporation.
Soomro, F. A., Haq, R. U., Al-Mdallal, Q. M., and Zhang, Q. (2018). Heat generation/absorption and nonlinear radiation effects on stagnation point flow of nanofluid along a moving surface. Results in physics, 8, 404-414. https://doi.org/10.1016/j.rinp.2017.12.037
Swain, K., Ibrahim, S. M., Dharmaiah, G., and Noeiaghdam, S. (2023). Numerical study of nanoparticles aggregation on radiative 3D flow of maxwell fluid over a permeable stretching surface with thermal radiation and heat source/sink. Results in Engineering, 19, 101208. https://doi.org/10.1016/j.rineng.2023.101208
Swarna J. B. A., Lavanya, B., Vijaya, K., and Murugiah, M. (2024). Effects of Arrhenius activation energy on thermally radiant Williamson nanofluid flow over a permeable stretching sheet with viscous dissipation. Journal of Advanced Research in Fluid Mechanics and Thermal Sciences, 118(2), 181–195. https://doi.org/10.37934/arfmts.118.2.181195
Thabet, E. N., Khan, Z., Abd-Alla, A. M., and Bayones, F. S. (2025). Thermal enhancement, thermophoretic diffusion, and Brownian motion impacts on MHD micropolar nanofluid over an inclined surface: numerical simulation. Numerical Heat Transfer, Part A: Applications, 86(4), 871-890.. https://doi.org/10.1080/10407782.2023.22
Uddin, M. J. (2011). Convective flow of micropolar fluids along an inclined flat plate with variable electric conductivity and uniform surface heat flux. Daffodil international university journal of science and technology, 6(1), 69-79. https://doi.org/10.3329/diujst.v6i1.9336
Reddy, M. V., and Lakshminarayana, P. (2021). Cross-diffusion and heat source effects on a three-dimensional MHD flow of Maxwell nanofluid over a stretching surface with chemical reaction. The European Physical Journal Special Topics, 230(5), 1371-1379. https://doi.org/10.1140/epjs/s11734-021-00037-9
Roja, P., Sankar Reddy, T., Mohammed Ibrahim, S., Parvathi, M., Dharmaiah, G., and Lorenzini, G. (2024). Magnetic field influence on thermophoretic micropolar fluid flow over an inclined permeable surface: a numerical study. Journal of Applied and Computational Mechanics, 10(2), 369-382. https://doi.org/10.22055/JACM.2024.44739.4265
Younes, H., Mao, M., Murshed, S. S., Lou, D., Hong, H., and Peterson, G. P. (2022). Nanofluids: Key parameters to enhance thermal conductivity and its applications. Applied Thermal Engineering, 207, 118202. https://doi.org/10.1016/j.applthermaleng.2022.118202
Zeeshan, A., Mehmood, O. U., Mabood, F., and Alzahrani, F. (2022). Numerical analysis of hydromagnetic transport of Casson nanofluid over permeable linearly stretched cylinder with Arrhenius activation energy. International Communications in Heat and Mass Transfer, 130, 105736. https://doi.org/10.1016/j.icheatmasstransfer.2021.105736